Int. J. Heat Mass Transfer. Vol. 23, pp. 1471–1478

0017-9310/80/1101-1471 $02.00/0

# EFFECT OF SURFACE TENSION ON CONDENSATE MOTION IN LAMINAR FILM CONDENSATION (STUDY OF LIQUID FILM IN A SMALL TROUGH)

SHIGEKI HIRASAWA*, KUNIO HIJIKATA†, YASUO MORI† and WATARU NAKAYAMA*

(*Received* 2 *January* 1980 *and in revised form* 31 *March* 1980)

**Abstract**—This study reveals that, on a finned surface, there exists a region of high heat transfer coefficients in the trough between the crests of fins. A theoretical analysis had predicted a local thinness of the condensate film produced by the capillary action in the trough. This is confirmed by optical measurements of the film thickness in a flow of ethyl alcohol along the model vertical walls. The results of this experiment agree well with the theoretical prediction. Taking these effects into account, the performance of a vertical finned surface is computed using condensation of R-113 and water.

## NOMENCLATURE

$d$, hydraulic diameter of condensate liquid in region C of Fig. 2 [m];
$e$, thickness of liquid film at trough bottom [m];
$G$, liquid flow rate in region C of Fig. 2 or 9 [$m^3/s$];
$G_t$, total volume of condensate in trough [$m^3/s$];
$g$, acceleration of gravity [$m/s^2$];
$H$, height of heat transfer surface [m];
$h$, half of a width of trough [m];
$L$, specific latent heat [J/kg];
$l$, depth of trough or half of a width of open channel [m];
$n$, refractive index;
$p$, pressure [$N/m^2$];
$r$, leading edge radius of fin [m];
$S$, value of $\eta$ at surface of fin [$m^{1/2}$];
$T$, temperature [K];
$t$, time [s];
$u$, velocity in $x$ direction [m/s];
$v$, velocity in $y$ direction [m/s];
$x$, gravitational direction [m];
$y$, horizontal direction on the surface of trough or at the bottom of open channel [m];
$z$, direction normal to the fin surface [m];
$\alpha$, condensation heat transfer coefficient [$W/m^2K$];
$\Delta T$, temperature difference between vapor and condensing surface [K];
$\delta$, thickness of liquid film [m];
$\delta_l$, thickness of film at $y = l$ in Fig. 9 [m];
$\delta_e$, thickness of film at $y = l - e - \varepsilon$ in Fig. 2 or at $y = l - \varepsilon$ in Fig. 9 [m];
$\delta_\eta$, thickness of film in $\eta$ co-ordinate [$m^{1/2}$];
$\varepsilon$, length of parabolic part of region C in Fig. 2 and 9 [m];
$\theta$, angle of refraction;
$\eta, \xi$, parabolic co-ordinate [$m^{1/2}$];
$\lambda$, thermal conductivity [W/mK];
$\mu$, viscosity [kg/ms];
$\rho$, density [$kg/m^3$];
$\psi$, inclination of liquid film surface;
$\sigma$, surface tension [N/m].

Subscripts
$s$, saturated vapor;
$w$, condensing surface.

## 1. INTRODUCTION

FILM condensation heat transfer has been widely used in power generating cycles, refrigerators, air-conditioners, chemical plants and many other cooling devices of industrial use. Many methods [1] for enhancing condensation heat transfer have been proposed. Among them, Gregorig [2] first recognized the importance of surface tension in film condensation on vertical fluted tubes. Thereafter many experimental studies [3–5] on fluted surfaces were made to confirm his findings. Contrasted to most of those previous studies which gave emphasis on fluted surfaces having rather round crests and troughs, there is a report [6] pointing out that a heat transfer surface, if provided with a number of small sharp fins, will have a very high condensation heat transfer coefficient. In the authors' view, the following two effects of surface tension will be main contributors to this phenomenon. Firstly, the surface tension works near the top of a fin resulting in a very thin film, thereby decreasing the thermal resistance there. Secondly, the surface tension by condensation in the trough induces a strong suction flow near the side surface of a fin, tending to produce a region of very thin liquid film. The authors' previous report [7] dealt with the first effect, specifically the effect of surface tension on a single vertical fin with a sharp crest, and analyzed the optimum radius of curvature of the fin's crest. This paper focuses on the

* Mechanical Engineering Research Laboratory, Hitachi Limited, Tsuchiura, Ibaragi, Japan.
† Tokyo Institute of Technology, Meguro, Tokyo, Japan.

suction effect brought about by the condensate in the trough. The relevant previous works are those of Karkhu *et al.* [8] and Rifert *et al.* [9], who made the analyses assuming that the pressure gradient caused by surface tension was constant along the surface of a fin. In the present analysis no such assumption is adopted, and it is going to be pointed out that a variable pressure gradient could produce a locally thin liquid film on the side surface of a fin. Recently Fujii *et al.* [10] analyzed condensation on a vertical surface of sinuous fins, but did not point out the possibility of enhancement discussed here. The only paper which mentioned the formation of a locally thinned film was that of Edwards *et al.* [11], but it reported no detailed or quantitative results. In order to gain a clear insight of the phenomenon, a theoretical analysis is attempted on a flow of condensate along a vertical finned surface. The result of the analysis is then confirmed by experiments. The experimental model is designed to make visual observation of a liquid film on a vertical open channel.

## 2. THEORETICAL ANALYSIS OF CONDENSATION ON A VERTICAL FINNED SURFACE

Prediction of condensation on a vertical finned surface as shown in Fig. 1 is our ultimate purpose. However, to simplify the analysis, a trapezoidal cross section of a real trough is approximated by a rectangular cross section as shown in Fig. 2. As the trough is of a symmetric shape, only a half of the cross section is considered. The co-ordinates are $x$ in the gravitational direction, $y$ in the horizontal direction along the fin surface and $z$ in the direction perpendicular to the fin surface. The trough depth is $l$ and the trough width $2h$.

A side surface of the trough is divided into three regions: a region near the crest of the fin (region A, Fig. 2), that near the bottom (region C) and an intermediate region (region B).

In the theoretical analysis, the following assumptions are made.

(1) The vapor is pure and saturated, and the viscous shear of the vapor on the liquid film is negligible. The temperature of the condensing surface is constant and the Marangoni effect is negligible.

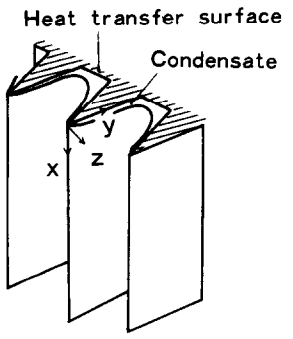


FIG. 1. Vertical finned surface.

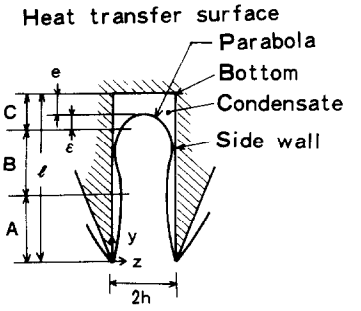


FIG. 2. Cross section of a trough.

(2) The inertia and convective terms in the fundamental equations are small compared with the viscous, gravity and conduction terms.

(3) The liquid film is thin in the regions A and B, so that changes of velocity and temperature in the $x$ and $y$ directions are small compared with those in $z$ direction. The boundary layer approximation can be applied.

(4) The variation of the liquid–vapor interface in the $x$ direction is much smaller than that in the $y$ direction in the regions A and B.

(5) The contour of the liquid–vapor interface in the region C can be regarded as a circular arc in view of the dominant effect of surface tension. In the analysis it is expressed by a parabolic function to ensure smooth transition with the interface in the region B.

(6) Following the previous report [7], the crest part of the fin (region A) is assumed to be of a parabolic shape with a small leading edge radius, and to have a finite film thickness even in the vicinity of the fin edge.

Using the above assumptions, fundamental equations for the liquid flow in the region B are written as

$$\mu\frac{\partial^2 u}{\partial z^2} + \rho g = 0 \tag{1}$$

$$\mu\frac{\partial^2 v}{\partial z^2} - \frac{\partial p}{\partial y} = 0 \tag{2}$$

$$\lambda\frac{\partial^2 T}{\partial z^2} = 0 \tag{3}$$

$$\frac{\partial}{\partial x}\int_0^\delta u\,dz + \frac{\partial}{\partial y}\int_0^\delta v\,dz = \frac{\lambda}{L\rho}\left[\frac{\partial T}{\partial z}\right]_{z=\delta}. \tag{4}$$

Equation (1) is the momentum equation in the $x$ direction, equation (2) in the $y$ direction, equation (3) the energy equation and equation (4) relates the increase of condensed liquid to the heat flux across the liquid film.

On the fin surface ($z = 0$), the boundary condition is written as

$$u = 0, \quad v = 0, \quad T = T_w. \tag{5}$$

On the liquid–vapor interface ($z = \delta$),

(i) no shear stress

$$\frac{\partial u}{\partial z} = 0, \quad \frac{\partial v}{\partial z} = 0, \tag{6}$$

(ii) saturated state of the vapor

$$T = T_s, \tag{7}$$

(iii) continuity of normal stress

$$p = -\frac{\sigma(\partial^2\delta/\partial y^2)}{[1 + (\partial\delta/\partial y)^2]^{3/2}} + p_s. \tag{8}$$

Equations (1)–(3) are integrated with the aid of the boundary conditions (5)–(8), and combined with equation (4) to obtain the following equation (9) for the thickness of the liquid film $\delta$.

$$\frac{\rho g}{3\mu}\frac{\partial\delta^3}{\partial x} + \frac{\sigma}{3\mu}\frac{\partial}{\partial y} \times \left[\delta^3\frac{\partial}{\partial y}\left\{\frac{\partial^2\delta/\partial y^2}{[1 + (\partial\delta/\partial y)^2]^{3/2}}\right\}\right] = \frac{\lambda\Delta T}{\rho L}\frac{1}{\delta}. \tag{9}$$

The first term of the left side is the flow rate drawn by gravity to the $x$ direction, the second term the flow rate drawn by surface tension to the $y$ direction, and the right side corresponds to the condensing rate. Here $\Delta T = T_s - T_w$.

Another form of integral equation is written here to facilitate the analysis for the region close to the fin crest. Following the analytical procedure in the previous report [7], equation (9) is rewritten in terms of parabolic co-ordinates $(x, \xi, \eta)$ and thickness $\delta_\eta$. (It is noted that there is a difference in postures of the fin relative to gravity in [7] and in the present case. A vertical two-dimensional fin with a top leading edge around which condensate flows downward due to gravity is assumed in [7], whereas the present fin extends its crest line in the vertical direction. Therefore, the gravity term in equation (10) differs from that in [7]).

$$\frac{\rho g}{3\mu}(\xi^2 + S^2)^{3/2}\frac{\partial\delta_\eta^3}{\partial x} + \frac{\sigma}{3\mu}\frac{1}{\sqrt{(\xi^2 + S^2)}}\frac{\partial}{\partial\xi} \times \left\{\delta_\eta^3\left[\sqrt{(\xi^2 + S^2)}\frac{\partial^3\delta_\eta}{\partial\xi^3} - \frac{3\xi^2}{(\xi^2 + S^2)^{3/2}}\frac{\partial\delta_\eta}{\partial\xi} + \frac{3\xi(S + \delta_\eta)}{(\xi^2 + S^2)^{3/2}}\right]\right\} = \frac{\lambda\Delta T}{\rho L}\frac{1}{\sqrt{(\xi^2 + S^2)}\delta_\eta}. \tag{10}$$

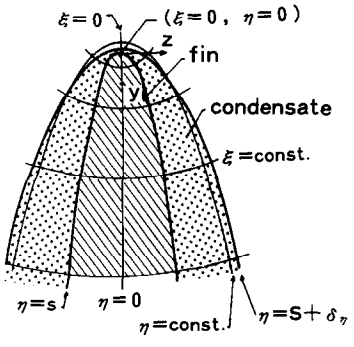


FIG. 3. Parabolic co-ordinates for crest part of fin.

In the region C, $\delta$ is approximated by a parabola as explained in assumption (5):

$$\delta = h - (h - \delta_\varepsilon)\sqrt{[(l - e - y)/\varepsilon]}, \tag{11}$$

where $\delta_\varepsilon$ is the film thickness at the boundary between the regions B and C ($y = l - e - \varepsilon$), $e$ the film thickness at the trough bottom and $\varepsilon$ the length of the transition zone in the region C, as shown in Fig. 2. The boundary between the regions B and C is not well defined on a real fin, but can be set arbitrarily so as to facilitate the analysis. To do this, the value of $\varepsilon$ is set as $\varepsilon = (l - e)/10$. After computations with different values of the denominator within a physically plausible range, the value of 10 is chosen because the deviation from this value introduces only a minor modification in the final result. For example, the use of 6 instead of 10 brings only about 5% change in the prediction of condensation on a typical fin. As the flow in the region C is assumed to be laminar and vertically oriented, the wall friction coefficient is $64\mu/\rho\bar{u}d$. Where $\bar{u}$ is the mean velocity and $d$ the hydraulic diameter of the liquid film. Then the volume flow rate $G$ in the region C is given as

$$G = (\rho g/\mu)[e^3h^3/(e + h)^2]. \tag{12}$$

This volume flow rate $G$ is equal to the total flow rate of condensate flowing horizontally into the region C from the region B,

$$G = 2\int_0^x \frac{\sigma}{3\mu}\left[\delta^3\frac{\partial}{\partial y}\left\{\frac{\partial^2\delta/\partial y^2}{\left[1 + \left(\frac{\partial\delta}{\partial y}\right)^2\right]^{3/2}}\right\}\right]_{y=l-\varepsilon} \mathrm{d}x. \tag{13}$$

The boundary between the region A and B in Fig. 2 is set at $y = (l - e - \varepsilon)/2$. This definition is rather arbitrary, but could be justified as a compromise of placing the boundary well spaced from both the fin tip and the trough bottom. Some of the assumptions and equations described above provide the boundary conditions for the regions A and B.

Zero film thickness at the top of the heat transfer surface,

$$x = 0\colon\ \delta = 0,\ \delta_\eta = 0. \tag{14}$$

The symmetry condition of condensate at the crest of the fin,

$$\xi = 0\colon\ \frac{\partial\delta_\eta}{\partial\xi} = 0,\ \frac{\partial^3\delta_\eta}{\partial\xi^3} = 0. \tag{15}$$

Smooth connection of $\delta$ between the regions A and B to the third derivatives,

$$y = \frac{l - e - \varepsilon}{2},\quad \xi = \sqrt{(S^2 + l - e - \varepsilon)}\colon$$

$$\delta = \sqrt{(\xi^2 + S^2)}\delta_\eta$$

$$\frac{\partial\delta}{\partial y} = \frac{S + \xi_\eta + \xi(\partial\delta_\eta/\partial\xi)}{\xi - (S + \delta_\eta)(\partial\delta_\eta/\partial\xi)}$$

$$\frac{\partial^2\delta}{\partial y^2} = \frac{[\xi^2+(\delta_\eta+S)^2]\dfrac{\partial^2\delta_\eta}{\partial\xi^2} + \left[\xi-(\delta_\eta+S)\dfrac{\partial\delta_\eta}{\partial\xi}+\xi\left(\dfrac{\partial\delta_\eta}{\partial\xi}\right)^2\right]\dfrac{\partial\delta_\eta}{\partial\xi} - (S+\delta_\eta)}{[\xi-(S+\delta_\eta)(\partial\delta_\eta/\partial\xi)]^3}$$

$$\delta^2\frac{\partial}{\partial y}\left\{\frac{\partial^2\delta/\partial y^2}{\left[1+\left(\dfrac{\partial\delta}{\partial y}\right)^2\right]^{3/2}}\right\} = \delta_\eta^2\left[\frac{\partial^3\delta_\eta}{\partial\xi^3} - \frac{3\xi^2}{(\xi^2+S^2)^2}\frac{\partial\delta_\eta}{\partial\xi} + \frac{3\xi(S+\delta_\eta)}{(\xi^2+S^2)^2}\right]. \quad (16)$$

Smooth connection of $\delta$ between the regions B and C to the second derivatives,

$$y = l-e-\varepsilon: \quad \frac{\partial\delta}{\partial y} = \frac{h-\delta_\varepsilon}{2\varepsilon}, \quad \frac{\partial^2\delta}{\partial y^2} = \frac{h-\delta_\varepsilon}{4\varepsilon^2}. \quad (17)$$

Under these boundary conditions, equations (9)–(13) are numerically integrated. The heat transfer coefficient is defined in terms of the base area of the heat transfer surface and the total volumetric flow rate $G_t$ of condensed liquid in the trough,

$$\alpha = \frac{\rho L G_t}{2hH\Delta T}, \quad (18)$$

where $\Delta T$ is the temperature difference between the vapor and the fin surface, $H$ the height of the heat transfer surface and $L$ the latent heat. Details of the results will be discussed later, but the noteworthy film thickness distribution is depicted in Fig. 2. The liquid film is locally thin near the boundary between the regions B and C. This is due to a large pressure gradient in the $y$ direction generated by the surface tension and the resistance against the liquid flow towards the trough bottom. Such a locally thin film should be an important contributor to the enhancement of heat transfer heretofore left without close attention by other investigators. However, it is difficult to confirm the calculated shape of liquid film by an experiment with real condensing fins because the fin size is too small to make any sensible measurements. To circumvent the difficulty, the experiment was planned with an enlarged model without condensation taking place on the fin surfaces, namely, letting the liquid (ethyl alcohol) flow down the model fin surfaces. The underlying notion is that locally thin films are the direct consequence of the pulling force in the trough liquid while the mass transfer of condensation bears little direct influence upon the physical process. Therefore, observation of the lateral ($y$ direction) flow and the distribution of the film thickness on the enlarged model would suffice for the proof of the analytical result.

## 3. EXPERIMENT

### 3.1. *Experimental apparatus*

The outline of the experimental apparatus is shown in Fig. 4. A wide vertical rectangular open channel is cut away in an acrylic plate. Its width varies from 11 mm at the top to 2 mm at the bottom in order to simulate the increasing condensate flow. The wide flat surface corresponds to the fin's side surface, and each tapered surface of 1.9 mm wide corresponds to a half of the trough bottom. The geometry should be viewed as formed by separating the finned surface at the middle of the trough and making both halves butt at the fin tips.

Liquid is supplied from an overhead tank to be pulled toward the corners as it flows down the cut-open channel. The tank containing a large quantity of ethyl alcohol is installed about 500 mm above the acrylic plate. The liquid passes through a narrow rectangular space of about 0.1 mm gap at the top of the acrylic plate to form a thin film downward. Ethyl alcohol is used as liquid, which easily forms filmwise flow. The thickness of the liquid film on the symmetry line ($y = 0$) is measured by a micrometer. The shape of the liquid film is measured by utilizing the refraction on striped light beams on the liquid surface. The beams produced by a Mach–Zehnder interferometer with a He–Ne laser are shed from the backside of the acrylic plate. In Fig. 5 the method of measurement is explained in a horizontal cross section. The beam A is taken up for illustration. When no liquid film is in the cut-open channel, the beam A goes straight through the acrylic plate and arrives at the point C on the screen. Consequently, the exact stripes of source light are reproduced on the screen. An example of such stripes is shown in Fig. 6(a). The acrylic surfaces, except the channel surfaces, are painted in black to facilitate observation. When liquid flows in the channel, the beam A is refracted in proportion to the angle of incidence on the liquid film surface (B) and arrives at the point D on the screen. An example of such stripes is shown in Fig. 6(b). The refracted angle $\theta$ can be obtained by $\theta = \tan^{-1}(\mathrm{CD/BC})$, where BC is the distance between the liquid film and the screen, and CD is the distance of stripe shift on the screen. There is a relation, $\sin(\psi+\theta)/\sin\psi = n$, between the angle of

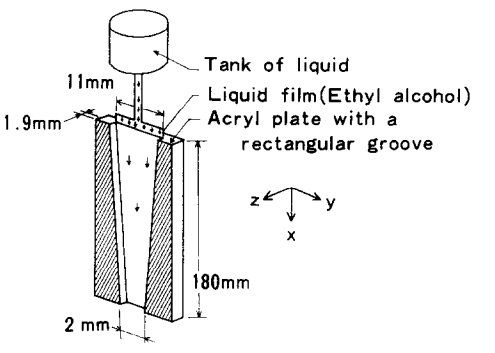


FIG. 4. Experimental apparatus.

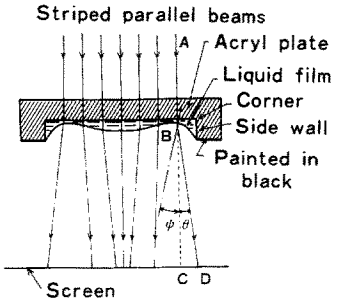


FIG. 5. Measurement of distribution of liquid film thickness.

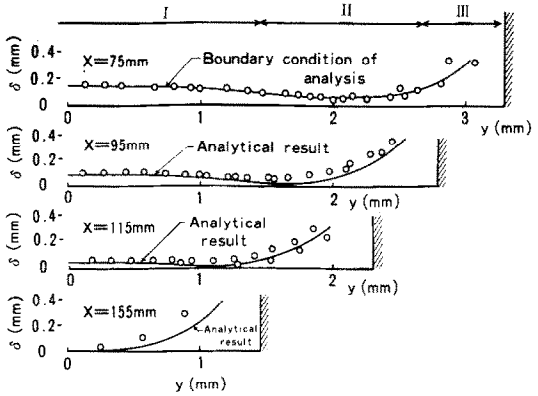


FIG. 7. Liquid film thickness.

incidence on the film surface $\psi$ and the refracted angle $\theta$, where $n$ is the refractive index of the liquid. The angle of incidence $\psi$ can be determined by this equation. The narrower stripe shape in the center part of Fig. 6(b) indicates the liquid film being convex, and the wider stripe shape in the both sides indicates the film surface being concave. The distribution of the liquid film thickness is thus determined by combining the distribution of $\psi$ and the measured thickness of the liquid film on the symmetric line ($y = 0$). Measurement errors are estimated as $\pm 0.05$ mm in $\delta$, and $\pm 0.2$ mm in determination of the lateral ($y$) location. The flow direction in the liquid film is measured by a particle tracking method using aluminum powders of 1 $\mu$m particle dia.

### 3.2 *Experimental results*

Figure 7 shows the results of measurement of the liquid film thickness in the cross sectional planes of $x = 75$ mm, 95 mm, 115 mm and 155 mm from the top. Because of symmetry, only a half of each cross section is shown. Refraction is very large near the side wall and the accuracy of measurement deteriorates there. Each figure shows thickening of the liquid film near the corner (region III). A flow towards the corner is generated by the surface tension, and the liquid film becomes thin locally (region II), for example, at $y = 2.1$ mm and $x = 75$ mm. Going downstream to $x = 95$ mm and 115 mm, the channel becomes narrower, and the points of locally thin liquid film approach the line of symmetry. At $x = 155$ mm the thinnest liquid film is seen on the line of symmetry.

Figure 8 shows the results of observation on the flow direction in the liquid film. It is seen that the liquid flows downstream near the line of symmetry (region I) and the corners (region III), but almost horizontally in region II.

## 4. COMPARISON OF THEORETICAL PREDICTION WITH EXPERIMENTAL RESULTS

### 4.1. *Theoretical analysis*

A theoretical analysis is made to find the film thickness distribution exactly compatible with the

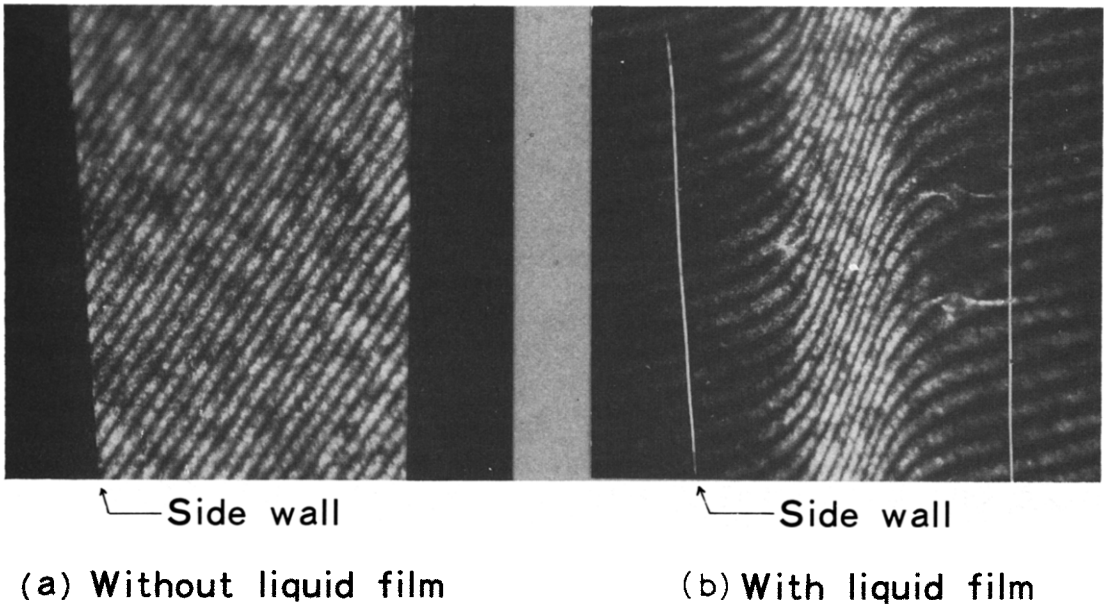


FIG. 6. Examples of stripes on screen.

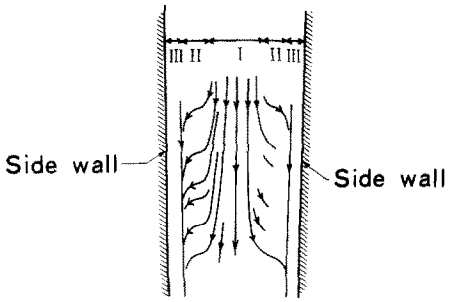


FIG. 8. Observed flow direction in liquid film.

situation of the model experiment using the same method as expounded in section 2. Co-ordinates ($x$, $y$, $z$) are as shown in Figs 4 and 9. The equation for the thickness $\delta$ is identical with equation (9). However, because of no phase change in the present experiment, the temperature difference between the vapor and the condensing surface is set as $\Delta T = 0$. The measured thickness of the film at $x = 75$ mm is taken as the initial condition for marching integration in the $x$ direction.

The boundary conditions are

$$y = 0: \quad \frac{\partial \delta}{\partial y} = 0, \quad \frac{\partial^3 \delta}{\partial y^3} = 0 \tag{19}$$

$$y = l - \varepsilon: \quad \frac{\partial \delta}{\partial y} = \frac{\delta_l - \delta_\varepsilon}{2\varepsilon}, \quad \frac{\partial^2 \delta}{\partial y^2} = \frac{\delta_l - \delta_\varepsilon}{4\varepsilon^2}, \tag{20}$$

where $\delta_\varepsilon$ is the liquid thickness at the boundary between the regions B and C ($y = l - \varepsilon$), $\delta_l$ at the side wall ($y = l$), $l$ half the width of the cut-open channel and $\varepsilon$ the length of the region C. From the experimental distributions in Fig. 7, it is seen that the liquid film within a distance of 0.4 mm from the side wall of the channel is particularly thick. Consequently $\varepsilon$ is set to be 0.4 mm. The flow rate in the $x$ direction in the corner is determined by referring to the velocity distribution in the corner calculated by Fulford [12]. Figure 9 depicts the flow regions in the corner (E–I) where velocity distributions are expressed by approximate formulae.

The velocity distributions in the regions G and I are assumed to be similar on lines perpendicular to the solid surface, and on any such line, the distribution is approximated by a quadratic function which is identical to the velocity distribution in a liquid film having same film thickness but infinite lateral extent. The velocity distribution in the quadrant region H is written by direct interpolation of the distributions in G and I. Namely, using the cylindrical co-ordinate whose axis is set at D, the distribution on the line DE is rewritten to be assumed to hold in the quadrant region. In the region F, liquid is assumed to be stagnant. From these approximate formulae, the total volumetric flow rate in the corner (C) is computed as

$$G = \frac{\rho g}{\mu}\left\{\frac{\pi}{16}(\mathrm{DE})^4 + \frac{\varepsilon^3}{21}\frac{(\delta_l - \mathrm{DE})^7}{(\delta_l - \delta_\varepsilon)^6} + \frac{\delta_l^3}{3}(\varepsilon - \mathrm{DE})\right.$$

$$- \frac{2\delta_l^2}{3\sqrt{\varepsilon}}(\delta_l - \delta_\varepsilon)[\varepsilon^{3/2} - (\mathrm{DE})^{3/2}]$$

$$+ \frac{\delta_l}{2\varepsilon}(\delta_l - \delta_\varepsilon)^2[\varepsilon^2 - (\mathrm{DE})^2]$$

$$\left. - \frac{2}{15\varepsilon^{3/2}}(\delta_l - \delta_\varepsilon)^3[\varepsilon^{5/2} - (\mathrm{DE})^{5/2}]\right\}. \tag{21}$$

Here,

$$\mathrm{DE} = \delta_l + \frac{(\delta_l - \delta_\varepsilon)^2}{3\varepsilon} - \sqrt{\left(\frac{\delta_l(\delta_l - \delta_\varepsilon)^2}{\varepsilon} + \frac{(\delta_l - \delta_\varepsilon)^4}{4\varepsilon^2}\right)}. \tag{22}$$

Measured film configurations in Fig. 7 reveal that the configurations in the corner are almost invariant in the $x$ direction. Therefore, equation (21) is assumed to hold all the way from at $x = 75$ mm downward. Corresponding to equation (13), G is also rewritten as the rate of influx to the region C from B.

$$G = \int_0^x \frac{\sigma}{3\mu}\left\{\delta^3 \frac{\partial}{\partial y}\left(\frac{\partial^2 \delta / \partial y^2}{\left[1 + \left(\frac{\partial \delta}{\partial y}\right)^2\right]^{3/2}}\right)\right\}_{y = l - \varepsilon}. \tag{23}$$

### 4.2. *Numerical calculation*

Integration of equation (9) is made by employing a backward difference scheme in the $x$ direction and a central difference scheme in the $y$ direction. Finite different meshes are given to the spacing of 10 mm in

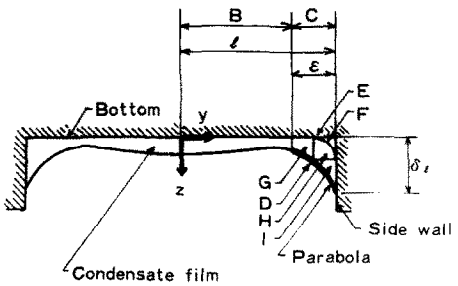


FIG. 9. Cross section of a cut-open channel.

the $x$ direction and an equal partition of 10 in the $y$ direction. Calculations are also made by changing the mesh size to 5 mm in the $x$ direction, and the results are in agreement with those for 10 mm spacing within 5% deviations. Integration proceeds from $x = 75$ mm, and at each horizontal location, $\delta$, $\delta_\varepsilon$, $\varepsilon_l$ and $G$ are obtained from equations (9), (21), (22) and (23) by iteration. When the value of the difference between the right and left sides of equation (9) becomes less than $10^{-3}$ times each term, a solution is assumed to be obtained.

### 4.3. *Comparison between analytical and experimental results*

In Fig. 7 analytical results are shown by solid lines. These are in good agreement with the experimental results. The minimum thickness of the liquid film at $x = 155$ mm is about 5 $\mu$m. Figure 10 shows a distribution of the local velocity of the liquid averaged in the film thickness at $x = 95$ mm. In the neighborhood of the line of symmetry (region I) the liquid flows down vertically by gravity, but in the region of locally thin film (region II) the liquid moves in the horizontal direction due to surface tension in the corner, and in the corner region the drainage velocity is very large. These features agree with the results of observation shown in Fig. 8.

## 5. ANALYTICAL RESULTS OF CONDENSATION ON A FINNED SURFACE

Having confirmed the existence of locally thin films and the plausibility of the present analysis. The effect of fin geometry upon condensation heat transfer is surveyed with R-113 and water. The results are shown in Figs. 11 and 12, respectively. Calculations are made for heat transfer surfaces of 50 mm long, assuming that the temperature difference between the vapor and the condensing surface is as $\Delta T = 10$ K, the fin height $l = 0.9$ mm, the fin thickness negligible, and the trough width $2h$ taken as the abscissae of Figs. 11 and 12 is identical with the fin pitch. The leading edge radius of the fin's crest ($r = s^2$) is assumed to be $10^{-5}$ m, because the heat transfer coefficients on the fins whose leading edge radii are less than $10^{-5}$ m are practically independent of the edge radius according to our previous report [7]. The heat transfer coefficients in these figures are studies on the trough with an area of $2h \times 50$ mm$^2$. The contribution by the surface area increase is shown by A in Fig. 11. When Nusselt correlation is used, the average heat transfer coefficient for a vertical finless surface of 50 mm long is found to be 1.6 kW/m$^2$K for water. This times the surface area increase produces the upper line of A.

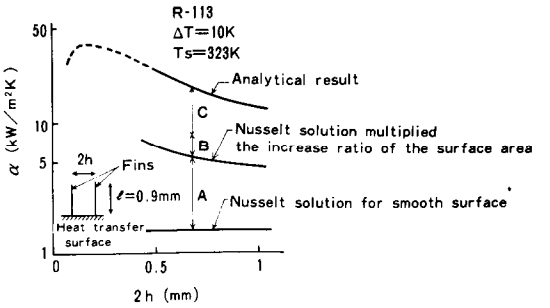


FIG. 11. Condensation performance of finned surface (R-113).

Addition of the effect of surface tension on the crest of the fin pushes up the heat transfer coefficients by an amount indicated by B, in this example 1.5 times the Nusselt prediction. Further, the effect of thin films studied in this report makes a significant contribution as indicated by C. The combined contribution of B and C reaches a value between 3–3.5 times the Nusselt prediction, being a little insignificant for the design of high performance condensation surfaces. However, further decrease of the trough width causes flooding there resulting in serious reduction in heat transfer coefficients. This suggests that the maximum average heat transfer coefficient is achieved at a certain trough width which is a little narrower than 0.5 mm for the case of Fig. 11. However, to obtain the optimum condition for film condensation along a vertical finned surface a more accurate analysis of flow is required. Such analysis using a more realistic geometry of fins and their thermal conductivity will be reported in future.

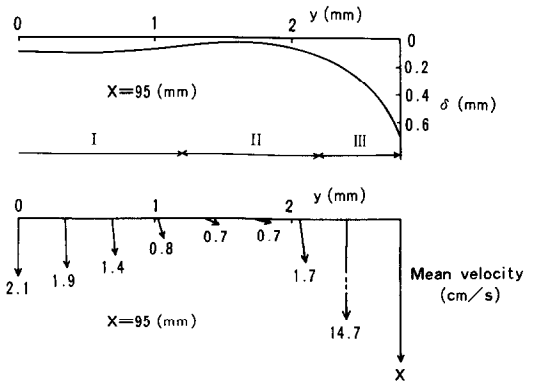


FIG. 10. Flow direction and velocity of liquid.

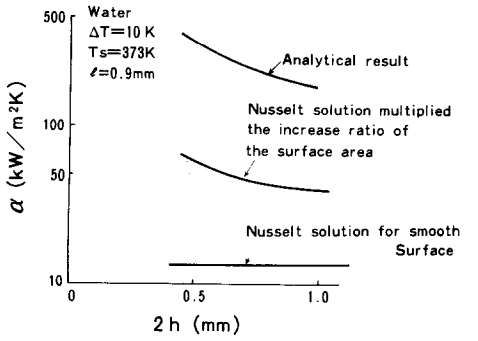


FIG. 12. Condensation performance of finned surface (water).

## 6. CONCLUSION

From the present study the following conclusions are obtained.

(1) The liquid film near the bottom of a narrow trough becomes locally thin. This is caused by the suction of the liquid flowing into the trough and makes a substantial contribution to the enhancement of condensation heat transfer.

(2) Quantitative estimation of contribution by the surface tension effects is carried out on an example finned surface having fins 0.9 mm high. The combined effects due to the fin crest and the trough liquid raises the heat transfer coefficients to 3–3.5 times the Nusselt prediction. It is suggested that both fins and trough being smaller than those previously considered are preferable for enhancement of condensation heat transfer.

(3) The present prediction is based on the model experiment in which the film of ethyl alcohol flows on a vertical open channel. Existence of locally thin film is confirmed, and the theoretical prediction of film thickness distributions is also confirmed to agree well with the experimental data.

## REFERENCES

1. A. G. Williams, S. S. Nandapurkar and F. A. Holland, A review of methods for enhancing heat transfer rate in surface condensers, *Chem. Engr, Lond.* **233**, CE367–CE373 (1968).
2. R. Gregorig, Hautkondensation an feingewellten Oberflächen bei Berücksichtigung der Oberflächenspannungen, *Z. Angew. Math. Phys.* **V**, 36–49 (1954).
3. K. Nabavian and L. A. Bromley, Condensation coefficient of water, *Chem. Engng Sci.* **18**, 651–660 (1963).
4. E. L. Lustenader, R. Richter and F. J. Neugebauer, The use of thin films for increasing evaporation and condensation rates in process equipment, *J. Heat Transfer* **81C**, 297–307 (1959).
5. T. C. Carnavos, Thin-film distillation, *Proceedings of First International Symposium on Water Desalination*, SWD-17 Washington (1965).
6. W. Nakayama, T. Daikoku, H. Kuwahara and K. Kakizaki, High-flux heat transfer surface "THERMOEXCEL", *Hitachi Rev.* **24**, 329–334 (1975).
7. S. Hirasawa, K. Hijikata, Y. Mori and W. Nakayama, Effect of surface tension on laminar film condensation along a vertical plate with a small leading radius, *Proceedings of the Sixth International Heat Transfer Conference*. Vol. 2, pp. 413–418 Toronto, Canada (1978).
8. V. A. Karkhu and V. P. Borovkov, Film condensation of vapor at finely finned horizontal tubes, *Heat Transfer Soviet Res.* **3**, 183–191 (1971).
9. V. G. Rifert, P. A. Barabash, A. B. Golubev, G. G. Leont'yev and S. I. Chaplinskiy, Investigation of film condensation enhanced by surface forces, *Heat Transfer — Soviet Res.* **9**, 23–27 (1977).
10. T. Fujii and H. Honda, Laminar filmwise condensation on a vertical single fluted plate, *Proceeding of the Sixth International Heat Transfer Conference*, Vol. 2, pp. 419–424 (1978).
11. D. K Edwards, K. D. Gier, P. S. Ayyaswamy and I. Cotton, Evaporation and condensation in circumferential grooves on horizontal tubes, ASME Publication 73-HT-25 (1973).
12. G. D. Fulford, The flow of liquids in thin films, *Adv. Chem. Engng* **5**, pp. 151–236 (1974).

## EFFET DE LA TENSION INTERFACIALE SUR LA CONDENSATION EN FILM LAMINAIRE (ETUDE D'UN FILM LIQUIDE DANS UN AUGET)

**Résumé**—Cette étude montre que, sur une surface ailetée, il existe une région à fort cefficient de transfert de chaleur dans la gorge entre les crêtes des ailettes. Une analyse théorique a déterminé la minceur locale d'un film de condensat produit par la capillarité dans l'auget. Ceci est confirmé par des mesures optiques de l'épaisseur de film dans un écoulement d'alcool éthylique le long des parois verticales. Les résultats de cette expérimentation s'accordent bien avec la prévision théorique. Prenant ces effets en compte, la performance d'une surface verticale ailetée est calculée en utilisant la condensation de R 113 et de l'eau.

## DER EINFLUß DER OBERFLÄCHENSPANNUNG AUF DIE KONDENSATSTRÖMUNG BEI LAMINARER FILMKONDENSATION (UNTERSUCHUNG DES FLÜSSIGKEITSFILMS IN EINER ENGEN RILLE)

**Zusammenfassung**—Die Untersuchung zeigt, daß es auf einer berippten Oberfläche ein Gebiet hoher Wärmeübergangskoeffizienten in der Rille zwischen den Rippenspitzen gibt. Aufgrund einer theoretischen Untersuchung war örtlich eine von Kapillarkräften in der Rille verursachte sehr geringe Dicke des Kondensatfilms vorausgesagt worden. Das wurde durch optische Messungen der Filmdicke in einer Äthylenströmung an senkrechten Modellwänden bestätigt. Die Ergebnisse dieses Experiments stimmen gut mit den theoretischen Voraussagen überein. Unter Berücksichtigung dieser Einflüsse wurde die Leistung einer senkrechten berippten Oberfläche für R 113 und Wasser berechnet.

## ВЛИЯНИЕ ПОВЕРХНОСТНОГО НАТЯЖЕНИЯ НА ДВИЖЕНИЕ КОНДЕНСАТА ПРИ ЛАМИНАРНОЙ ПЛЕНОЧНОЙ КОНДЕНСАЦИИ. ИССЛЕДОВАНИЕ ЖИДКОЙ ПЛЕНКИ В КЮВЕТЕ НЕБОЛЬШОГО РАЗМЕРА

**Аннотация** — Проведенное исследование свидетельствует о том, что в зазорах на оребренной поверхности наблюдаются высокие коэффициенты теплообмена. С помощью теоретического анализа показано, что в отдельных местах пленка конденсата, перемещающаяся под действием капиллярных сил в зазоре, имеет малую толщину. Это подтверждается оптическими измерениями толщины пленки при обтекании вертикальных стенок модели этиловым спиртом. Результаты экспериментов хорошо согласуются с данными теоретических расчетов. На примере конденсации R-113 и воды рассчитана эффективность вертикальной оребренной поверхности.